Research Article

Low Temperature Sintering Al-B Doped-LLZO for All-Solid-State Lithium Battery

Fitria Rahmawati*
Research Group of Solid-State Chemistry & Catalysis, Chemistry Department, Faculty of Mathematic and Natural Sciences, Sebelas Maret University, Surakarta, Indonesia

Imam Shofid Alaih
Department of Materials Engineering and Convergence Technology, Gyeongsang National University, Jinju, Gyeongnam, Republic of Korea

Hartoto Nursukatmo, Hanida Nilasari, Soraya Muzayanza, Mohamad Firdaus Armaka and Edo Raihan
R & D Refinery - PT. PERTAMINA (Persero), Pulogadung Jakarta Timur, Indonesia

* Corresponding author. E-mail: fitria@mipa.uns.ac.id DOI: 10.14416/j.asep.2024.09.006
Received: 27 May 2024; Revised: 29 July 2024; Accepted: 7 August 2024; Published online: 9 September 2024

Abstract
This research synthesizes a double Al-B doped LLZO following a composition of $Li_{7+0.5x}La_{1.14}Al_{1.43x}B_{0.5x}Zr_{2-3x}O_{12-\delta}$ through a solid-state reaction. The materials were sintered at a low temperature of 900 °C, giving an advantage in reducing Li loss. The material was analyzed to understand the phase content, the crystal structure and cell parameters, the surface morphology, the impedance, the electrical conductivity, and the activation energy for ionic migration. As a result, the Al-B doped-LLZO with x composition of 0.3 ($Li_{7.15}La_{1.14}Al_{0.429}B_{0.15}Zr_{1.1}O_{12-\delta}$) and ball milling time of 120 h, LLZBAO(0.3)120 h, provides the highest ionic conductivity of 6.898×10^{-4} Scm^{-1} at room temperature, and it increases as the temperature increases confirming activation energy of 0.135 eV. A prototype of LCO-LLZBAO(0.3)120h-Li metal battery was produced and tested to investigate the solid electrolyte performance. A cyclic voltammetry analysis confirms a quasi-reversible reaction involving extraction-insertion of Li ions into $LiCoO_2$. However, the excess capacity and a long plateau at low voltage also indicate the reduced Li^+ into zero valent-metal, which is poorly reversible, causing the battery capacity to decrease and become stable after 20 cycles.

Keywords: Al-B doped-LLZO, Solid electrolyte, Li metal battery, LLZO based electrolyte, LLZBAO

1 Introduction

Lithium batteries are widely used because of their high current and voltage densities, long cycle life, and their environmentally friendly [1], [2]. However, the liquid electrolyte application deals with the issues of explosion risk, less safety for transportation [1], [3], poor thermal stability, and high reactivity toward Li metal [4]. It reduces the potential use of Li metal anode, even though Li metal anode provides a high energy densities with a theoretical capacity of 3860 mAh/g and a low negative potential of metallic lithium anode (–3.04 V vs standard hydrogen electrode) [4]–[6]. Therefore, solid electrolyte is a good option to overcome the problems because of their non-flammable properties, high energy, and power density [7], better compatibility with Li metal anode compared to liquid electrolyte [8], and less growth of Li dendrite on the interface of electrolyte-electrode [9], [10].

Some solid electrolytes have been investigated, such as lithium superionic conductor, Li_3PO_4 (LISICON)[11], Lithium titanate perovskite-type [12], sodium superionic conductor (NASICON) [13], and garnet-type $Li_7La_3Zr_2O_{12}$[14]. The cubic garnet Lithium Lanthanum Zirconate ($Li_7La_3Zr_2O_{12}$, LLZO) is getting more attention due to its good electrochemical performance with ionic conductivity in the range of 10^{-4}–10^{-3} Scm^{-1}, and low electronic

conductivity [15], good thermal and chemical stability to Li metal, and has a large electrochemical window (~ 6 V) [16], [17]. To obtain a cubic LLZO at room temperature, some researchers modified LLZO with Al^{3+} [18], Ga^{3+} [19], Sm^{3+} [20], and Ta^{5+} [21] doping [22]. The Al^{3+} dopant stabilizes cubic structure, and reduces the cubic transformation to a tetragonal phase [23], and also increases the ionic conductivity because of Li vacancy formation [24], [25]. Meanwhile, Boron, B^{3+}, doping to LLZO could decrease the sintering temperature to 900 °C because of liquid phase formation between particles, allowing the particle arrangement. Low-temperature material preparation is essential to prevent Li loss that degrades their electrochemical performance [22]. The boron doping to LLZO has successfully produced ASS-LIB with a voltage range of 2.2–4.7 V at 1C of current drawn [26].

Based on the capability of Al^{3+} to stabilize the LLZO cubic phase [18], [27] and increase the ionic conductivity [24], [25] and the capability of B^{3+} to reduce the sintering temperature [28], a previous study on Al-B doping into LLZO was conducted by following a non-stoichiometric formula of $Li_{7+x}La_3B_{0.5x}Al_{0.5x}Zr_{2-x}O_{12}$ at various x of 0.15; 0.2; 0.4; and 0.7 [29]. XRD analysis equipped with Le Bail refinement found the presence of cubic phase at around 82%. However, secondary phases of $LiCO_3$, H_3BO_3, and $LiOH.H_2O$ are also available. After sintering at 1100 °C 6 h, the green pellet densified; however, it turned into powder after being stored at room temperature for 12 h [29]. It seems that the presence of 4% B promoted boric acid, H_3BO_3, formation, which caused the material to be hygroscopic and turned into powder quickly after being stored at ambient conditions.

Therefore, to overcome the hygroscopic problem due to a high B composition, this research applied a different formula of $Li_{7+0.5x}La_{1.14}Al_{1.43x}B_{0.5x}Zr_{2-3x}O_{12-\delta}$. The formula was chosen based on previous research conducted on Al^{3+} doping in LLZO [25]. Meanwhile, to prevent Li loss during sintering, a low- temperature sintering of 900 °C was chosen [24]. Low-temperature sintering also allows the sintering of the material without mother powder because less possibility of Li loss would not require Li compensation. This research applied 12 h, 100 h, and 120 h ball milling times to get high purity by reducing the presence of secondary phases.

The result was characterized by PXRD followed by Le Bail refinement to understand their crystal phases. The structure, cell parameters, and mole percentage. Impedance analysis of the prepared materials reveals their electric properties under various temperatures. Finally, this research studies the feasibility of the prepared material as a solid electrolyte in a lithium metal battery by assembling the prepared Al-B doped-LLZO (LLZABO) with $LiCoO_2$ cathode and Li anode. The battery performance was tested through charge-discharge analysis. Meanwhile, cyclic voltammetry analyzes electrochemical reactions within the battery.

2 Method and Materials

2.1 *Synthesis of the LLZBAO*

The material was synthesized by conventional solid-state reaction method according to a formula of $Li_{7+0.5x}La_{1.14}Al_{1.43x}B_{0.5x}Zr_{2-3x}O_{12-\delta}$ (LLZBAO) with composition of x= 0.3; 0.6. The precursors were LiOH (99%, Merck), La_2O_3 (95%, Merck), ZrO_2 (99%, MSE), B_2O_3 (99.98%, Sigma Aldrich), and $Al(OH)_3$ (99%, Merck). Prior to use, the La_2O_3 and $Al(OH)_3$ were heated at 900 °C for 12 h, meanwhile LiOH and ZrO_2 were heated at 200 °C for 12 h. The precursors were weighed stoichiometrically and then mixed thoroughly in isopropyl alcohol, followed by ball-milling at 450 rpm for 12 h. 10 wt% of LiOH was added to the mixture to compensate the potential lithium loss during calcination and sintering. After ball milling, the powder was separated from zirconia balls and added to the ball milling tube, which served as a powder crusher. The separated powder was heated in an oven at 70 °C for 12 h followed by calcination at 900 °C for 12 h. The calcined powder was then crushed in an agate pestle and pressed under 5 t (Hydraulic press, Mezler max.12 t) to produce a green pellet. The green pellets were sintered at 900 °C for 12 h under air without mother powder, producing LLZBAOO(0.3) and LLZABO(0.6).

The produced powder was then analyzed by PXRD (Rigaku miniflex 600 Cu-ray) equipped with Le Bail refinement (Rietica, a free version) to investigate the phase inside and fitted with a definite-crystal structure and cell parameters [30], [31]. The XRD patterns were merged and processed with OriginPro 2023 Serial No. GF3S5-6089-7181518, Reg.ID 8ZK-ZT7-L7K. The surface morphology of the powder was investigated by SEM-EDX (JEOL-JSM-6510LV). The SEM images were analyzed by ImageJ (a free software) to understand the pore's percentage and roughness [32]. Impedance analysis (EUCOL U-2826 frequency 20 Hz–5 MHz)

investigated the electrical properties [33]. Then, the prepared composition with higher ionic conductivity was further studied by applying different ball milling times of 12 h, 100 h, and 120 h. All the resulting powders were subjected to PXRD to investigate the phase content available.

2.2 *Electrochemical analysis*

The material was subjected to a 5-t hydraulic press and then sintering at 900 °C 12 h under air without mother powder. Impedance analysis at 20 Hz–5 MHz was done through the silver blocking method by applying the silver paste and the silver wire on both surface of the sintered-pellet. The study was conducted at 30, 50, 100, and 125 °C. ZView software embedded in CS Studio 5 for Electrochemical Workstation fitted the impedance data based on the R-C network model. The ionic conductivity, σ (Scm^{-1}), was then calculated from resistance, R (Ω) value found by the fitting step by applying Equation (1), with *l* as the pellet thickness (cm), and *A* as the surface of the active area (cm^2). Surface active area, *A* is the area of silver paste cast on the sample.

$$\sigma = \frac{1}{\mathrm{R}}\frac{\mathrm{l}}{\mathrm{A}} \quad (1)$$

To investigate the electrochemical performance of the material as a solid electrolyte, the SE was assembled with $LiCoO_2$ (LCO) cathode and Li metal anode in a coin cell CR2032. The LLZBAO was polished until 1 mm thick with a sandpaper No. 500. The LCO powder was mixed with PVDF, NMP, and acetylene black at 80:10:10, respectively [20] and stirred for 1 h. The cathode slurry was then painted on the LLZBAO pellet and was kept in an argon glove box for 12 h. Then, Li was melted on the other side of LLZBAO. Cu foil was attached on the Li side, and Al foil was on the LCO side. After being punched, the coin cell was analyzed by cyclic voltammetry (Corrtest Electrochemical Workstation CS-150, scan rate of 5 mVs^{-1}) and charge-discharge analysis with NEWARE Battery Testing System 1A5V under 1.2–3.8 V of 0.1C current drawn.

3 Result and Discussion

3.1 *X-Ray diffraction*

In this research, the LLZBAO was synthesized in two compositions of x = 0.3 and x = 0.6. Initially, the synthesis was conducted with 12 h of ball milling producing LLZBAO(0.3)12h and LLZBAO(0.6)12h. The powder provides XRD patterns, as shown in Figure 1.

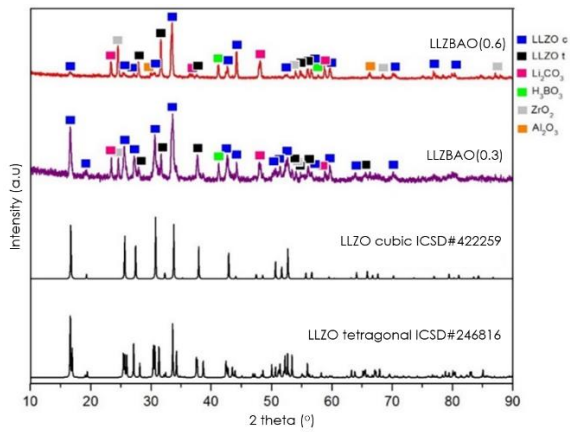

Figure 1: The diffraction patterns of LLZBAO(0.3)12 h and LLZBAO(0.6)12 h, which are compared with cubic LLZO ICSD#422259 and tetragonal LLZO ICSD#246816

Table 1: List of molar percentages, and cell parameters of the LLZO phase and the secondary phase in LLZBAO.

Composition LLZABO (x=)	**x = 0.3**	**x = 0.6**
LLZO *c* (mol%)	46.84	45.46
LLZO *t* (mol%)	46.31	45.72
Cell Parameter :		
LLZO *c*	cubic/	cubic/
Structure/*space group*	(*Ia-3d*)	(*Ia-3d*)
a=b=c (Å)	13.0165 (21)	12.9940 (10)
LLZO *t*	Tetragonal/	Tetragonal/
Structure /*space group*	(*I4/acd*)	(*I4/acd*)
a=b≠c (Å)	13.1226 (16)	13.1950 (15)
	12.6621 (22)	12.6446 (16)
Rp (%)	9.41	11.38
Rwp (%)	9.90	12.25
Secondary phase (mol %)		
H_3BO_3	2.91	2.89
Li_2CO_3	2.48	2.42
ZrO_2	1.47	1.46
Al_2O_3	-	1.95

LLZBAO(0.3)12h shows cubic diffraction at 2θ 16.64°, 30.7°, 33.6°, and also tetragonal peak at 2θ of 31.65°. Meanwhile, LLZBAO(0.6)12h shows an intense peak at 2θ of 33.6° and 42.70° corresponds to cubic structure, and at 2θ of 31.65° refers to tetragonal structure. Le Bail refinement to the XRD data found that LLZBAO(0.6)12h provides lower mol% of cubic structure than LLZBAO(0.3)12 h, which is 45.46% and 46.84% for LLZBAO(0.6)12h and LLZBAO(0.3)12h,

respectively. Meanwhile, LLZBAO(0.6)12h has secondary phases, including H_3BO_3, Li_2CO_3, ZrO_2 and Al_2O_3, with a total composition of 8.71% (Table 1). The secondary phases are the precursors, which indicates that the reaction did not proceed completely. Therefore, an effort to homogenize the mixture is required, such as by increasing milling time.

3.2 *Conductivity of LLZBAO*

Impedance measurement analyzed the effect of composition on the ionic conductivity. The results are depicted in Figure 2. ZView analysis found that both prepared materials show ionic conductivity with capacitance of 5.96×10^{-9} F and 1.32×10^{-10} F for LLZBAO(0.3)12 h and LLZBAO(0.6)12 h, respectively (Table 2). It indicates that grain boundary conduction dominates the conduction mechanism, as the capacitance of ~0.1 pF refers to grain capacitance, ~1.4 nF refers to grain boundary capacitance, and more than 1 μF is electrolyte-electrode capacitance [34], [35].

Figure 2 shows that at room temperature, LLZBAO(0.3)12 h provides lower impedance than LLZBAO(0.6)12 h. The ionic conductivity calculation found a value of 5.656×10^{-5} Scm^{-1} for LLZBAO(0.3)12 h, and 6.25×10^{-6} Scm^{-1} for LLZBAO(0.6)12 h. The 0.6 composition shows an order lower than the 0.3 composition. The lower cubic content and higher secondary phases are responsible for the lower conductivity value (Table 2). The Cubic structure allows Li ions to migrate freely within the structure because Li ions in the cubic LLZO (LLZO c) structure only partially occupy 24 d tetrahedral (Td) and 48 g/96 h octahedral (Oh) sites. Meanwhile, in tetragonal LLZO (LLZO t), three different Li sites are fully occupied [36], leaving less space for Li ions to migrate and provide conductivity.

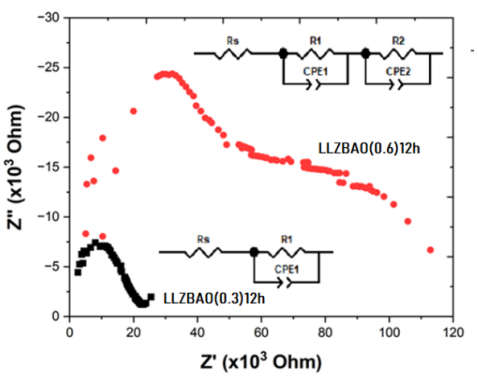

Figure 2: The impedance plots of LLZBAO(0.3)12 h and LLZBAO(0.6)12 h.

Table 2: Fit result of the impedance plots.

Sample	LLZBAO (0.3)12 h	LLZBAO (0.6)12 h
Thickness (cm)	0.101	0.222
Active area (cm^2)	0.067	0.214
R1 (Ω)	27147	54954
R2 (Ω)	-	51816
CPE1 (F)	5.96×10^{-9}	1.32×10^{-10}
CPE2 (F)	-	5.98×10^{-8}
Chi square	0.0186	0.0129
Ionic cond (Scm^{-1})	5.528×10^{-5}	9.703×10^{-6}

3.3 *SEM of LLZBAO(0.3) and LLZBAO(0.6)*

SEM images show that LLZBAO(0.3)12 h has larger grains (Figure 3(a) and (b)) than LLZBAO (0.6)12 h (Figure 3(c) and (d)). The LLZBAO(0.3)12 h grains are connected or well-sintered. Meanwhile, small grains of LLZBAO(0.6)12 h are poorly connected, which causes lower ionic conductivity. Figures 3(a) and (b) show that LLZBAO(0.3)12h has a spherical particle shape that sticks together and is tightly packed. Grains appear to be covered by a glassy layer. By increasing Al-B-dopants to x = 0.6, more pores are formed, and a melt or liquid phase is formed, resulting in intergranular connections (Figure 3(d)), which are often called abnormal grain growth[26]. Analysis by ImageJ software (a free software) found that LLZABO(0.3)12h provides a larger pore size of 7.501 ± 5.725 μm^2 than LLZBAO(0.6)12 h, i.e., 5.683 ± 3.674 μm^2. However, the pore number in LLZABO(0.3)12h is fewer than in LLZABO(0.6)12 h, with 0.88% and 1.99%, respectively (Figure 4). LLZBAO(0.3)12 h provides a smoother surface than LLZBAO(0.6)12 h (Figure 4).

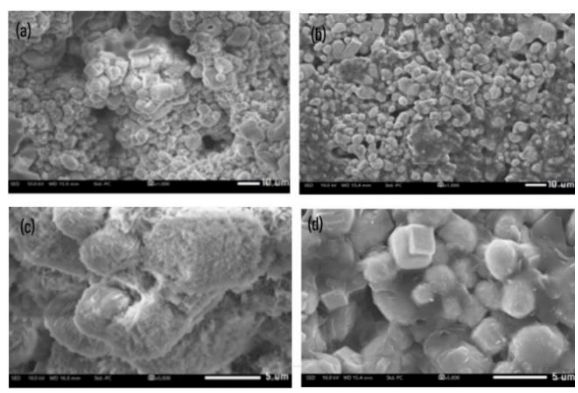

Figure 3: SEM images of LLZBAO(0.3)12 h (a), (b) and LLZBAO(0.6)12 h (c), (d) at different magnifications.

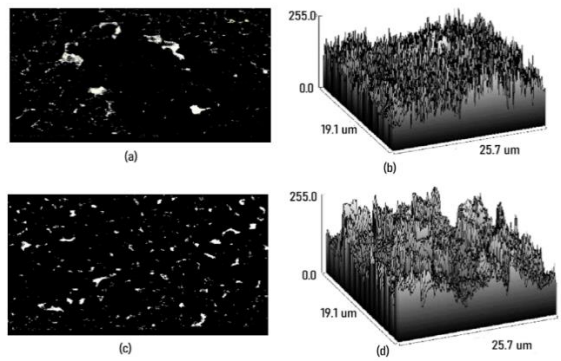

Figure 4: The ImageJ results of SEM images: (a) the pores of LLZBAO(0.3)12 h, (b) the roughness of LLZBAO(0.3)12 h, (c) the pores of LLZBAO(0.6)12 h, and (d) the roughness of LLZBAO(0.6)12 h.

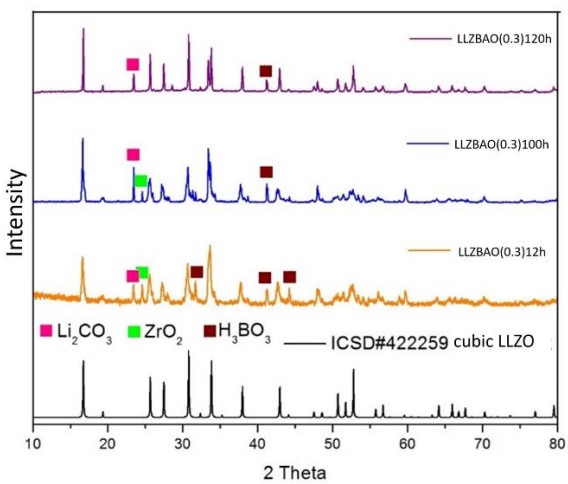

Figure 5: The diffraction patterns of LLZBAO (0.3)12 h, LLZBAO (0.3)100 h, and LLZABO (0.3)120 h.

The abnormal grain growth, as also found by previous research [26], is caused by a high grain boundary movement driven by a large amount of liquid phase. The larger grain boundary will engulf the smaller grain boundary to form much larger grains due to the large driving force of the curved boundary between the large grain and the matrix. Very high grain boundary movement rates will detach the boundaries of the pores and leave isolated pores in the interior of the grain because the pores move slower than the grain boundaries. Thus, the separation of these pore boundaries forms closed pores, causing abnormal growth grains [19], [26].

Considering the result, especially the ionic conductivity properties, this research further studied LLZBAO(0.3) for application tests. However, LLZBAO(0.3)12h still consists of many secondary phases of $LiCO_3$, H_3BO_3, ZrO_2, and Al_2O_3, which are identified as precursors. Incomplete mixing was predicted as the reason for the precursor's availability within the final product. Therefore, in this research, after having the suitable composition LLZBAO(0.3), which is $Li_{7.15}La_{1.14}Al_{0.429}B_{0.15}Zr_{1.1}O_{12-\delta}$, ball milling time was extended to 100 h and 120 h.

3.4 *Le Bail refinement of LLZBAO*

As shown previously, LLZABO(0.3) provided higher cubic content, lower pores percentage, and higher ionic conductivity. However, the material still consists of secondary phases of precursors, i.e., Li_2CO_3, H_3BO_3, ZrO_2, and Al_2O_3. Mechanical mixing is suspected to be the cause of some precursors remaining. Therefore, further treatment was done by applying a longer ball milling time of 100 h and 120 h. The resulting powder shows a diffraction pattern as depicted in Figure 5. Ball milling at 100 h reduced the peak intensity of the secondary phases. Furthermore, ball milling at 120 h made the diffraction peaks more intense and sharper (Figure 5) indicating high crystallinity. The zirconia peak was removed, while the Li_2CO_3 and H_3BO_3 are still available in minor peaks. The result is in line with other results in LLZO production which found that longer ball milling will increase the homogeneity of the starting material because it is able to provide a mechanical mix and chemical reactions among the starting materials to react more completely [37] without remaining ZrO_2 and $LaOH_3$ characteristic peaks [38].

Le Bail refinement (Figure 6) confirms that extending the ball milling time to 120 h could remove the ZrO_2 peak, and increase the cubic percentage to 89.63% (Table 3). It also reduces the cubic cell parameters from 13.046(2) Å to 12.9722(4) Å, indicating a lower unit cell volume without any disruption from the zirconia atom outside the LLZO structure. The map of electron distribution (Figure 6, inserted) shows that by eliminating ZrO_2 from the secondary phase, electrons were more evenly distributed, and the positive charge became connected to support ionic migration conveniently.

Table 3: Refinement result to LLZBAO (0.3)100h and LLZBAO(0.3)120 h.

Materials	Cell Parameter	Cubic	Secondary Phases		
			H_3BO_3	Li_2CO_3	ZrO_2
LLZBAO (0.3) 100h	*a* (Å)	13.046(2)	7.096(1)	8.377(2)	5.083(2)
	b (Å)	13.046(2)	7.053(2)	4.996(1)	5.249(1)
	c (Å)	13.046(2)	6.625(1)	6.218(1)	5.348(3)
	mole %	87.15(3)	5.45(0)	4.64(0)	2.76(0)
	Rp (%)		8.96		
	Rwp (%)		11.01		
Ionic conductivity (Scm^{-1})			5.528×10^{-5}		
LLZBAO (0.3) 120h	*a* (Å)	12.9722(4)	6.990(1)	8.315(1)	-
	b (Å)	12.9722(4)	6.993(1)	4.9804(9)	-
	c (Å)	12.9722(4)	6.6146(5)	6.1818(9)	-
	mole %	89.63(1)	5.59	4.78	-
	Rp (%)		8.90		
	Rwp (%)		8.83		
Ionic Conductivity (Scm^{-1})			6.898×10^{-4}		

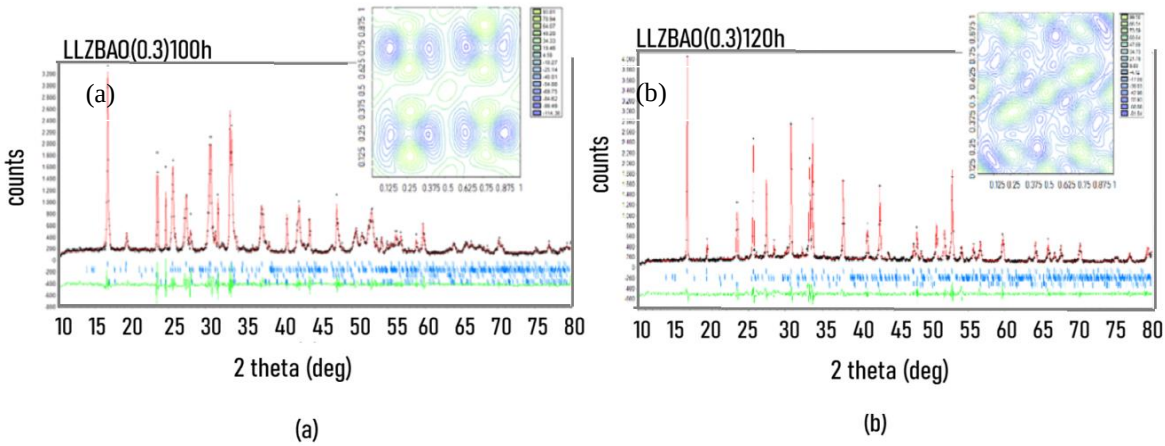

Figure 6: Le Bail and Fourier plots (inserted) of LLZBAO (0.3)100 h (a) and LLZBAO (0.3)120 h (b).

Table 4: Crystallyte size and lattice strain by Williamson-Hall method.

Materials	Crystallyte Size (nm)	Lattice Strain ($Å^2$)
LLZBAO(0.3) 12h	3.790 ± 1.868	0.037 ± 0.017
LLZBAO(0.6) 12h	7.159 ± 2.992	0.174 ± 0.007
LLZBAO(0.3) 100h	6.690 ± 3.989	0.020 ± 0.008
LLZBAO(0.3) 120h	7.165 ± 3.885	0.019 ± 0.008

The Williamson-Hall method evaluates crystallyte size and lattice strain of the prepared materials. The results are listed in Table 4. LLZBAO(0.6) shows the highest lattice strain of 0.174 ± 0.007 $Å^2$ confirming higher crystal imperfection such as by lattice dislocation [39].

Figure 7(a) shows an SEM image of LLZBAO(0.3)120h with cubic particles connected to each other, even though some connection losses are still available. ImageJ analysis (Figure 7(b)) found that LLZBAO(0.3)120 h has a smaller pore size of 3.265 ± 4.149 μm^2, but a larger pore number with 1.146% of pore percentage. The sintering temperature at 900 °C seems insufficient to completely dense the material. However, this research has chosen a low-temperature sintering to prevent Li loss that causes a decrease in Li^+ ion conductivity and eliminate the usage of mother powder during sintering.

Another research on compositing LLZO with NASICON type LATP also found that sintering at 800 °C provides higher electrical conductivity than sintering at 900 °C and above because a high temperature initiates high reactivity, allowing more secondary phases to form [15]. This research found that even though the sintered-pellet is not fully dense, as shown by Figure 7(a), however the high cubic

content and the absence of ZrO_2 as a secondary phase in LLZBAO(0.3)120 h (Table 3) has successfully increased the ionic conductivity from 5.528×10^{-5} Scm^{-1} for LLZBAO(0.3)12h (Table 2) to 6.898×10^{-4} Scm^{-1} for LLZBAO(0.3)120h at room temperature. Increasing the temperature even decreases the impedance value (Figure 8), indicating an increase in ionic conductivity.

3.5 *Ionic Conductivity of LLZO*

The impedance plots show wide semicircles indicating the presence of grain and grain boundary conduction, which was modeled by two R-CPE networks (inserted in Figure 8). The ionic conductivity of the LLZBAO(0.3)120 h is 6.898×10^{-4} Scm^{-1} at room temperature. The ionic conductivity increases as the temperature increases, i.e., 12.335×10^{-4} Scm^{-1}, 22.397×10^{-4} Scm^{-1}, and 30.043×10^{-4} Scm^{-1} at 50 °C, 100 °C, 125 °C, respectively. Arrhenius's plot confirms that the activation energy of the ionic movement is 0.153 eV. Table 5 lists some related LLZO-based solid electrolytes and shows the position of this research among them.

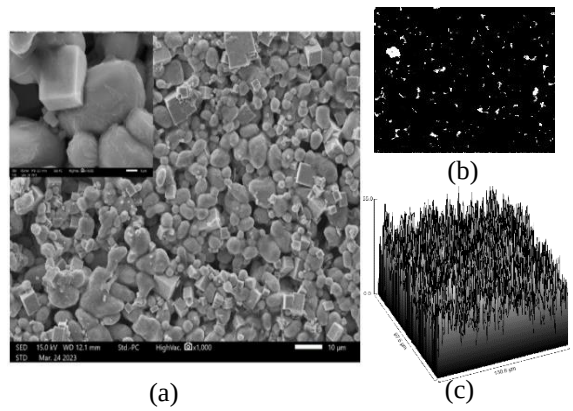

Figure 7: SEM Images of LLABAO(0.3)120 h (a) along with its imageJ pore analysis (b) and roughness (c).

Table 5: The ionic conductivity of some LLZO based-solid electrolyte

Materials	Sintering Method	Ionic Conductivity (Scm^{-1}) and the Reference
$Li_{6.8}La_3Zr_{1.9}Mo_{0.1}O_{12}$	1230 °C 4h in air	6.82×10^{-5} [40]
$Li_7La_3Zr_2O_{12}$	Double step sintering 900 °C / 6h then 1130 °C 18h	2.40×10^{-4} [41]
$Li_{6.75}La_3Zr_{1.75}Ta_{0.25}O_{12}$	Double step sintering 900 °C / 6h then 1130 °C 18h	4.30×10^{-4} [41]
$Li_{6.8}La_{2.95}Ba_{0.05}Zr_{1.75}Ta_{0.25}O_{12}$	Double step sintering 900 °C / 6h then 1130 °C 18h	6.50×10^{-4} [41]
$Li_{6.03}La_3Zr_{1.533}Ta_{0.46}O_{12}$	1000 °C /12h	5.21×10^{-6} [42]
$Li_7La_3Zr_{1.4}Ti_{0.6}O_{12}$	950 °C /12h	1.01×10^{-6} [42]
$Li_7La_3Zr_2O_{12}$	1200 °C /12h	1.2×10^{-6} [43]
$Li_7La_3Zr_2O_{12}$ sol-gel synthesis	1200 °C /12h	4.0×10^{-6} [43]
$Li_{6.25}Al_{0.25}La_3Zr_2O_{12}$	1200 °C /12h	8.9×10^{-5} [43]
Y-Al doped-LLZO	1050 °C /1h + 1200 °C /6h and CIP 40 MPa	1.06×10^{-5} [44]
B-Al doped-LLZO	900 °C /12 h in air	5.528×10^{-5} (this research)
B-Al doped-LLZO	900 °C /120 h in air	6.898×10^{-4} (This research)

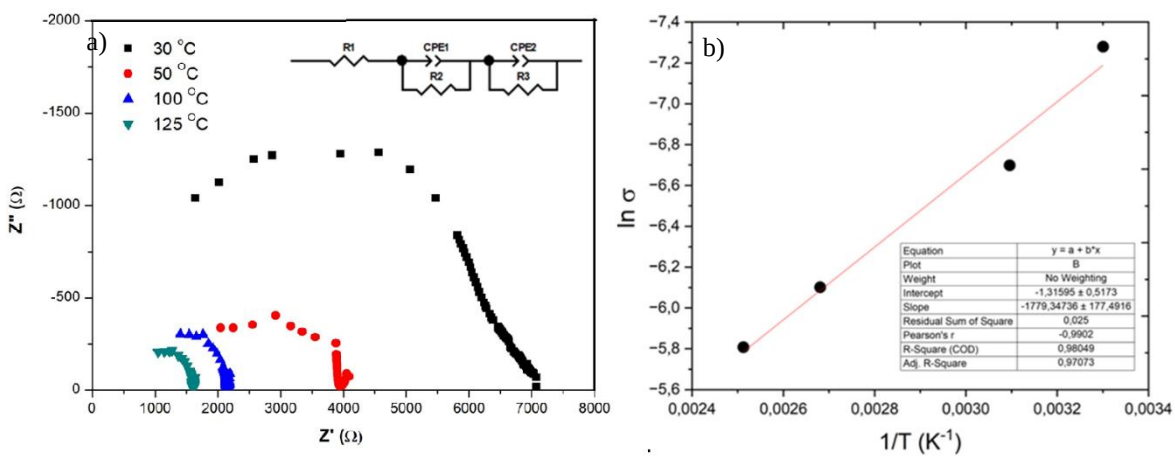

Figure 8: The impedance plots of LLZBAO(0.3)120 h at 30 °C, 50 °C, 100 °C and 125 °C (a), and its Arrhenius plot (b).

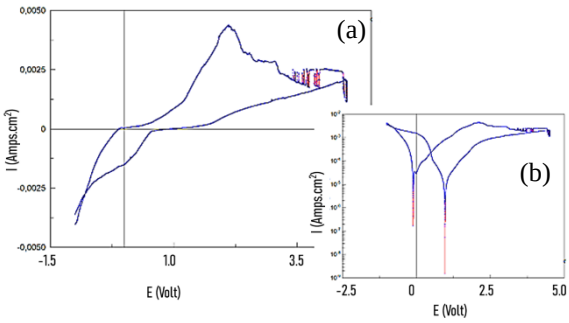

Figure 9: CV analysis of full cell LCO-LLZBAO(0.3)120 h-Li at 10 mV/s of scan rate vs Li/Li^+ (a). The inserted figure presents voltage vs log I clarifying the onset potential of anodic and cathodic reaction (b).

3.6 *Cyclic voltammetry*

Cyclic voltammetry to LCO-LLZBAO(0.3)120 h-Li found a quasi-reversible voltammogram confirming the reversible oxidation-reduction reaction. The oxidation started at 0.28 V vs Li/Li^+ and reached a maximum at 1.95 V vs Li/Li^+. The Li^+ was reversibly reduced at 0.3 V vs Li/Li^+ (Figure 9). The voltage vs. log i plot confirms a little shift between oxidation and reduction starting or onset potential, as inserted in Figure 9. The oxidation-reduction voltages are similar to another result on Au-Ta doped LLZO-Li, which shows 0 V vs. Li/Li^+ according to Li dissolution and Li deposition [45]. Another research on LCO-$Li_{6.75}La_3Zr_{1.75}Nb_{0.25}O_{12}$-Li solid-state battery found a similar oxidation start with a potential anodic peak at 3.8 V vs Li/Li^+ corresponds to Li ions intercalation to LCO [46].

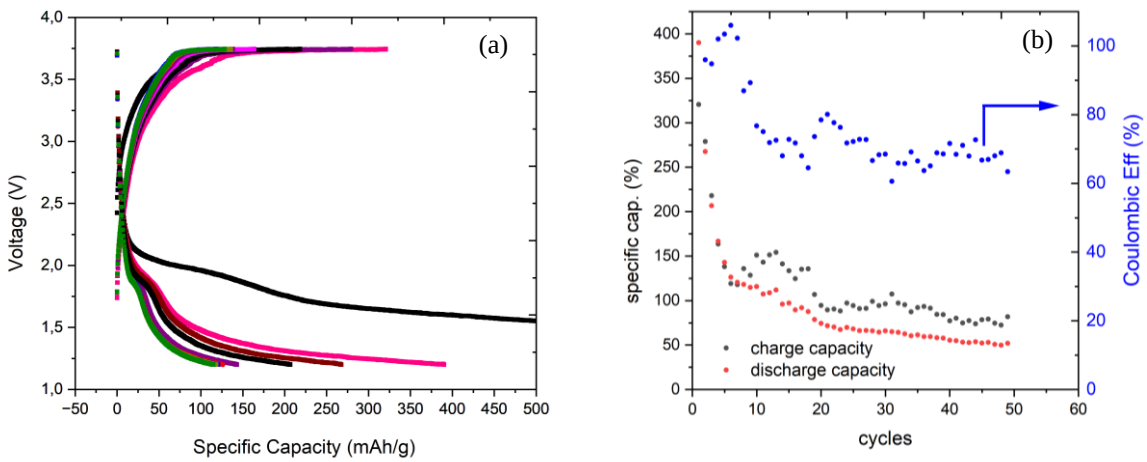

Figure 10: Charge-Discharge result (a) to LCO-LLZBAO(0.3)120h-Li under 0.1C current drawn, and its Coulombic Efficiency (b).

3.7 *Charge - Discharge*

Charge-discharge analysis to LCO-LLZBAO(0.3)120 h-Li found a very high initial discharge capacity of over 500 mAh/g (Figure 10), due to the transport of Li ions extracted from Li metal (theoretical specific capacity of 3860 mAh/g [47]) and transported to LCO as defined in Equation (2) based on an LCO-Carbon battery [48]. The second charge-discharged capacities are 325 mAh/g and 395 mAh/g, respectively, which notably exceeds the theoretical LCO capacity, i.e., 274 mAh/g for a 100% Li extraction. The surplus discharge capacity evinces Li^+ deposition to LCO (Equation (3)) was not only inserted to the LCO crystal structure with a maximum of $1.0Li^+$, but the excess of $0.5Li^+$ was deposited as zero-valent transition metal [49] on the LCO surface. Further investigation is essential to understand the case. A capacity surplus in another Li metal battery with LMF cathode ($Li_{1.2}MnFe_{1.2}F_{6.8}$) mostly occurs below 2.9 V as a gradient of discharge curve changed [49]. During the subsequent cycle, discharge capacity decreases to 128 mAh/g at the 10th cycle, providing 78% of Coulombic Efficiency (Figure 10). Disappearing of a long plateau under low voltage indicates that the zero-valent lithium deposited on LCO was poorly reversible [49]. After 20 cycles, the capacity remains stable at 100 mAh/g and discharged at around 70 mAh/g,

confirming an average efficiency of 75% (Figure 10). Another research on Al doped-LLZO analyzes stress-strain distribution and cracking phenomena within the solid electrolyte that impedes Li ions transport and reduces electrochemical performance [27].

Charging:
$LiCoO_2 \rightarrow Li_{1-n}CoO_2 + nLi^+ + ne$
$nLi^+ + ne \rightarrow Li_n$ (2)

Discharging:
$Li_n \rightarrow nLi^+ + ne$
$Li_{1-n}CoO_2 + nLi^+ + ne \rightarrow LiCoO_2$ (3)

4 Conclusions

Dual doping Al-B to LLZO produces a zirconia-based electrolyte mainly consisting of a cubic structure. The cubic content increases significantly by increasing the ball milling time to 120 h. A low sintering temperature of 900 °C 12 h in air without mother powder has successfully produced a solid electrolyte of LLZBAO(0.3)120h with a high ionic conductivity of 6.898×10^{-4} Scm^{-1} at room temperature. The prototype Li metal battery with LCO cathode and LLZBAO(0.3)120h electrolyte provides a quasi-reversible reaction at -1.5 V to 4.0 V vs Li/Li^+. The reaction is identified as the extraction-insertion of Li^+ to LCO. Charge-discharge analysis confirms that the battery initially shows an excess discharge capacity over theoretical LCO capacity, indicating a reduction to zero-valent lithium deposited on the LCO surface. The poor reversible zero-valent Li reduces the subsequent charge-discharge capacity until a stable value reached an average efficiency of 78%.

Acknowledgements

The Authors acknowledge The Ministry of Education, Culture, Research, and Technology, Republic of Indonesia, for funding this research under a scheme of PTUPT contract No. 673.1/UN27.22/PT.01.03/2022. The authors also acknowledge PT. Pertamina and Universitas Sebelas Maret who also support this research.

Author Contributions

F.R.: conceptualization, investigation, reviewing and editing; I.S.A.: investigation, methodology, data analysis; H.N.: funding acquisition; H.N.: data curation, administration; funding acquisition; S.M.: data curation; M.F.A.: data analysis; administration; E.R.: data analysis. All authors have read and agreed to the published version of the manuscript.

Conflicts of Interest

The authors declare no conflict of interest.

References

[1] K. B. Dermenci, A. F. Buluç, and S. Turan, "The effect of limonite addition on the performance of $Li7La_3Zr_2O_{12}$," *Ceramics International*, vol. 45, no. 17, pp. 21401–21408, 2019, doi: 10.1016/j.ceramint.2019.07.128.

[2] Z. Cao, X. Cao, X. Liu, W. He, Y. Gao, and J. Liu, "Effect of Sb-Ba codoping on the ionic conductivity," *Ceramics International*, vol. 41, no. 5, pp. 6232–6236, 2015, doi: 10.1016/j.ceramint.2015.01.030.

[3] L. Bai, W. Xue, Y. Li, X. Liu, Y. Li, and J. Sun, "The interfacial behaviours of all-solid-state lithium ion batteries," *Ceramics International*, vol. 44, no. 7, pp. 7319–7328, 2018, doi: 10.1016/j.ceramint.2018.01.190.

[4] C. Fang, X. Wang, and Y. S. Meng, "Key issues hindering a practical lithium-metal anode," *Trends in Chemistry*, vol. 1, no. 2, pp. 152–158, 2019, doi: 10.1016/j.trechm.2019.02.015.

[5] T. Wang, R. Zhang, Y. Wu, G. Zhu, C. Hu, J. Wen, and W. Luo, "Engineering a flexible and mechanically strong composite electrolyte for solid-state lithium batteries," *Journal of Energy Chemistry*, vol. 46, pp. 187–190, 2020, doi: 10.1016/j.jechem.2019.10.010.

[6] R. Xu, X.-Q. Zhang, X.-B. Cheng, H.-J. Peng, C.-Z. Zhao, C. Yan, and J.-Q. Huang, "Artificial soft-rigid protective layer for dendrite-free lithium metal anode," *Advanced Functional Materials*, vol. 28, no. 8, 2018, Art. no. 1705838, doi: 10.1002/adfm.201705838.

[7] K. V. Kravchyk, D. T. Karabay, and M. V. Kovalenko, "On the feasibility of all-solid-state batteries with LLZO as a single electrolyte," *Scientific Reports*, vol. 12, no. 1, pp. 1–10, 2022, doi: 10.1038/s41598-022-05141-x.

[8] J. Shen, S. Liu, D. Bian, Z. Chen, H. Pan, C. Yang, W. Tian, Y. Li, L. Kong, H. Quan, D.-W. Wang, and S. Zhu, "Efficient nanoarchitectonics of solid-electrolyte-interface for high-performance all-solid-state lithium metal batteries via mild

fluorination on polyethylene oxide," *Electrochimica Acta*, vol. 456, 2023, Art. no. 142482, doi: 10.1016/j.electacta.2023.142482.

[9] T. Ye, L. Li, and Y. Zhang, "Recent progress in solid electrolytes for energy storage devices," *Advanced Functional Materials*, vol. 30, no. 29, 2020, Art. no. 2000077, doi: 10.1002/adfm.202000077.

[10] J.-G. Zhang, W. Xu, J. Xiao, X. Cao, and J. Liu, "Lithium metal anodes with nonaqueous electrolytes," *Chemical Reviews*, vol. 120, no. 24, pp. 13312–13348, 2020, doi: 10.1021/acs.chemrev.0c00275.

[11] A. Neveu, V. Pelé, C. Jordy, and V. Pralong, "Exploration of Li–P–S–O composition for solid-state electrolyte materials discovery," *Journal of Power Sources*, vol. 467, pp. 2–8, 2020, doi: 10.1016/j.jpowsour.2020.228250.

[12] J. Lu, Y. Li, and Y. Ding, "Structure, stability, and ionic conductivity of perovskite Li2x-ySr1-x-yLayTiO$_3$ solid electrolytes," *Ceramics International*, vol. 46, no. 6, pp. 7741–7747, 2020, doi: 10.1016/j.ceramint.2019.11.277.

[13] S. Narayanan, S. Reid, S. Butler, and V. Thangadurai, "Sintering temperature, excess sodium, and phosphorous dependencies on morphology and ionic conductivity of NASICON $Na_3Zr_2Si_2PO_{12}$," *Solid State Ionics*, vol. 331, pp. 22–29, 2019, doi: 10.1016/j.ssi.2018.12.003.

[14] L. Shen, L. Wang, Z. Wang, C. Jin, L. Peng, X. Pan, J. Sun, and R. Yang, "Preparation and characterization of Ga and Sr co-doped $Li_7La_3Zr_2O_{12}$ garnet-type solid electrolyte," *Solid State Ionics*, vol. 339, 2019, Art. no. 114992, doi: 10.1016/j.ssi.2019.05.027.

[15] I. M. Hung and D. Mohanty, "Preparation and characterization of LLZO-LATP composite solid electrolyte for solid-state lithium-ion battery," *Solid State Communications*, vol. 364, no. 135, 2023, Art. no. 115135, doi: 10.1016/j.ssc.2023.115135.

[16] S. Kobi and A. Mukhopadhyay, "Structural (in)stability and spontaneous cracking of Li-La-zirconate cubic garnet upon exposure to ambient atmosphere," *Journal of the European Ceramic Society*, vol. 38, no. 14, pp. 4707–4718, 2018, doi: 10.1016/j.jeurceramsoc.2018.06.014.

[17] E. A. Il'ina, A. A. Raskovalov, and A. P. Safronov, "The standard enthalpy of formation of superionic solid electrolyte $Li_7La_3Zr_2O_{12}$," *Thermochimica Acta*, vol. 657, pp. 26–30, 2017, doi: 10.1016/j.tca.2017.09.019.

[18] R. H. Brugge, J. A. Kilner, and A. Aguadero, "Germanium as a donor dopant in garnet electrolytes," *Solid State Ionics*, vol. 337, pp. 154–160, 2019, doi: 10.1016/j.ssi.2019.04.021.

[19] J. Su, X. Huang, Z. Song, T. Xiu, M. E. Badding, J. Jin, and Z. Wen, "Overcoming the abnormal grain growth in Ga-doped $Li_7La_3Zr_2O_{12}$ to enhance the electrochemical stability against Li metal," *Ceramics International*, vol. 45, no. 12, pp. 14991–14996, 2019, doi: 10.1016/j.ceramint.2019.04.236.

[20] X. Wang, J. Liu, R. Yin, Y. Xu, Y. Cui, L. Zhao, and X. Yu, "High lithium ionic conductivity of garnet-type oxide Li7+xLa3Zr2-xSmxO12 (x = 0–0.1) ceramics," *Materials Letters*, vol. 231, pp. 43–46, 2018, doi: 10.1016/j.matlet.2018.08.006.

[21] Y. Gong, Z. G. Liu, Y. J. Jin, J. H. Ouyang, L. Chen, and Y. J. Wang, "Effect of sintering process on the microstructure and ionic conductivity of Li7–xLa3Zr2–xTaxO12 ceramics," *Ceramics International*, vol. 45, no. 15, pp. 18439–18444, 2019, doi: 10.1016/j.ceramint.2019.06.061.

[22] G. Kalita, T. Endo, and T. Nishi, "Recent development on low temperature synthesis of cubic-phase LLZO electrolyte particles for application in all-solid-state batteries," *Journal of Alloys and Compounds*, vol. 969, 2023, Art. no. 172282, doi: 10.1016/j.jallcom.2023.172282.

[23] P. Zhao, G. Cao, Z. Jin, H. Ming, Y. Wen, Y. Xu, X. Zhu, Y. Xiang, and S. Zhang, "Self-consolidation mechanism and its application in the preparation of Al-doped cubic $Li_7La_3Zr_2O_{12}$," *Materials and Design*, vol. 139, pp. 65–71, 2018, doi: 10.1016/j.matdes.2017.10.067.

[24] J. Li, Z. Liu, W. Ma, H. Dong, K. Zhang, and R. Wang, "Low-temperature synthesis of cubic phase $Li_7La_3Zr_2O_{12}$ via sol-gel and ball milling induced phase transition," *Journal of Power Sources*, vol. 412, pp. 189–196, 2019, doi: 10.1016/j.jpowsour.2018.11.040.

[25] Z. Hu, H. Liu, H. Ruan, R. Hu, Y. Su, and L. Zhang, "High Li-ion conductivity of Al-doped Li7La3Zr2O12 synthesized by solid-state reaction," *Ceramics International*, vol. 42, no. 10, pp. 12156–12160, 2016, doi: 10.1016/j.ceramint.2016.04.149.

[26] Y. Tang, Z. Luo, T. Liu, P. Liu, Z. Li, and A. Lu, "Effects of B_2O_3 on microstructure and ionic conductivity of Li6.5La3Zr1.5Nb0.5O12 solid

electrolyte," *Ceramics International*, vol. 43, no. 15, pp. 11879–11884, 2017, doi: 10.1016/j.ceramint.2017.06.035.

[27] J. Adjah, K. I. Orisekeh, R. A. Ahmed, M. Vandadi, B. Agyei-Tuffour, D. Dodoo-Arhin, E. Nyankson, J. Asare, N. Rahbar, and W. O. Soboyejo, "Cyclic-induced deformation and the degradation of Al-doped LLZO electrolytes in all-solid-state Li-metal batteries," *Journal of Power Sources*, vol. 594, 2024, doi: 10.1016/j.jpowsour.2023.234022.

[28] D. Uzun, "Boron-doped Li1.2Mn0.6Ni0.2O2 as a cathode active material for lithium ion battery," *Solid State Ionics*, vol. 281, pp. 73–81, 2015, doi: 10.1016/j.ssi.2015.09.008.

[29] I. S. Alaih, K. D. Nugrahaningtyas, F. Rahmawati, M. F. Armaka, H. Haeruddin, and H. Nilasari, "Crystal structure and morphology of B-Al doped-lithium lantanum zirconate," *AIP Conference Proceedings*, vol. 2391, 2022, doi: 10.1063/5.0072447.

[30] F. Rahmawati, S. Wahyuningsih, and D. Irianti, "The photocatalytic activity of SiO_2-TiO_2/graphite and its composite with silver and silver oxide," *Bulletin of Chemical Reaction Engineering and Catalysis*, vol. 9, no. 1, pp. 45–52, 2014, doi: 10.9767/bcrec.9.1.5374.45-52.

[31] E. G. Temam, A. Elkhanssa, H. B. Temam, F. Kermiche, and H. Bentrah, "The influence of arabic gum on the catalytic properties of Ni-Mo alloy coatings to intensify hydrogen evolution reaction," *Anti-Corrosion Methods and Materials*, vol. 64, no. 6, pp. 580–587, 2017, doi: 10.1108/ACMM-10-2016-1722.

[32] E. Guettaf Temam, F. Djani, S. Rahmane, H. Ben Temam, and B. Gasmi, "Photocatalytic activity of Al/Ni doped TiO_2 films synthesized by sol-gel method: Dependence on thickness and crystal growth of photocatalysts," *Surfaces and Interfaces*, vol. 31, 2022, Art. no. 102077, doi: 10.1016/j.surfin.2022.102077.

[33] L. Lemya, B. T. Hachemi, and G. T. Elhachmi, "Surface and electrochemical properties of electrodeposited Ni-WC nanocomposites coatings," *Main Group Chemistry*, vol. 64, no. 6, pp. 763–772, 2017.

[34] P. Martín, M. L. López, C. Pico, and M. L. Veiga, "Li(4-x)/3Ti(5-2x)/3CrxO4 ($0 \leq x \leq 0.9$) spinels: New negatives for lithium batteries," *Solid State Sciences*, vol. 9, no. 6, pp. 521–526, 2007, doi: 10.1016/j.solidstatesciences.2007.03.023.

[35] F. Rahmawati, N. Zuhrini, K. D. Nugrahaningtyas, and S. K. Arifah, "Yttria-stabilized zirconia (YSZ) film produced from an aqueous nano-YSZ slurry: Preparation and characterization," *Journal of Materials Research and Technology*, vol. 8, no. 5, pp. 4425–4434, 2019, doi: 10.1016/j.jmrt.2019.07.054.

[36] M. R. Bonilla, F. A. García Daza, J. Carrasco, and E. Akhmatskaya, "Exploring Li-ion conductivity in cubic, tetragonal and mixed-phase Al-substituted $Li_7La_3Zr_2O_{12}$ using atomistic simulations and effective medium theory," *Acta Materialia*, vol. 175, pp. 426–435, 2019, doi: 10.1016/j.actamat.2019.06.033.

[37] D. S. Aleksandrov, A. A. Popovich, W. Qingsheng, and P. A. Novikov, "Synthesis of tetragonal solid-state electrolyte $Li_7La_3Zr_2O_{12}$," *Materials Today: Proceedings*, vol. 30, pp. 587–591, 2019, doi: 10.1016/j.matpr.2020.01.142.

[38] J. K. Padarti, T. T. Jupalli, C. Hirayama, M. Senna, T. Kawaguchi, N. Sakamoto, N. Wakiya, and H. Suzuki, "Low-temperature processing of Garnet-type ion conductive cubic $Li_7La_3Zr_2O_{12}$ powders for high performance all solid-type Li-ion batteries," *Journal of the Taiwan Institute of Chemical Engineers*, vol. 90, 2018, doi: 10.1016/j.jtice.2018.02.021.

[39] A. Moradabadi and P. Kaghazchi, "Effect of lattice and dopant–induced strain on the conductivity of solid electrolytes: application of the elastic dipole method," *Materialia*, vol. 9, 2020, Art. no. 100607, doi: 10.1016/j.mtla.2020.100607.

[40] D. Rettenwander, A. Welzl, L. Cheng, J. Fleig, M. Musso, E. Suard, M. M. Doeff, G. J. Redhammer, and G. Amthauer, "Synthesis, crystal chemistry, and electrochemical properties of Li 7–2 x La 3 Zr 2– x Mo x O 12 (x = 0.1–0.4): Stabilization of the cubic garnet polymorph via substitution of Zr 4+ by Mo 6+," *Inorganic Chemistry*, vol. 54, no. 21, pp. 10440–10449, 2015, doi: 10.1021/acs.inorgchem.5b01895.

[41] Y. Meesala, Y. K. Liao, A. Jena, N.-H. Yang, W. K. Pang, S.-F. Hu, H. Chang, C.-E. Liu, S.-C. Liao, J.-M. Chen, X. Guo, and R.-S. Liu, "An efficient multi-doping strategy to enhance Li-ion conductivity in the garnet-type solid electrolyte $Li_7La_3Zr_2O_{12}$," *Journal of Materials Chemistry A*, vol. 7, no. 14, pp. 8589–8601, 2019, doi: 10.1039/c9ta00417c.

[42] M. Abreu-Sepúlveda, D. E. Williams, A. Huq, C. Dhital, Y. Li, M. P. Paranthaman, K. Zaghib, and A. Manivannan, "Synthesis and characterization

of substituted garnet and perovskite-based lithium-ion conducting solid electrolytes," *Ionics*, vol. 22, no. 3, pp. 317–325, 2016, doi: 10.1007/s11581-015-1556-2.

[43] J. Košir, S. Mousavihashemi, B. P. Wilson, E. L. Rautama, and T. Kallio, "Comparative analysis on the thermal, structural, and electrochemical properties of Al-doped $Li_7La_3Zr_2O_{12}$ solid electrolytes through solid state and sol-gel routes," *Solid State Ionics*, vol. 380, pp. 1–10, 2022, doi: 10.1016/j.ssi.2022.115943.

[44] S. K. Arifah, F. Rahmawati, and Y. Hidayat, "Cold isostatic pressing treatment in the preparation of Al and Y-Doped LLZO (Li6.15La3Zr1.75Al0.2Y0.25O12-δ) solid electrolyte," in *Recent Advances in Renewable Energy Systems, Select Proceeding of ICOME 2021*, pp. 231–239, 2022, doi: 10.1007/978-981-19-1581-9_26.

[45] Y. Zhang, J. Deng, D. Hu, F. Chen, and Q. Shen, "Electrochimica acta synergistic regulation of garnet-type Ta-doped Li 7 La 3 Zr 2 O 12 solid electrolyte by Li þ concentration and Li þ transport channel size," *Electrochimica Acta*, vol. 296, pp. 823–829, 2019, doi: 10.1016/j.electacta.2018.11.136.

[46] W. Guo, F. Shen, J. Liu, Q. Zhang, H. Guo, Y. Yin, J. Gao, Z. Sun, X. Han, and Y. Hu, "In-situ optical observation of Li growth in garnet-type solid state electrolyte," *Energy Storage Materials*, vol. 41, pp. 791–797, 2021, doi: 10.1016/j.ensm.2021.07.023.

[47] W. Xu, J. Wang, F. Ding, X. Chen, E. Nasybulin, Y. Zhang, and J.-G. Zhang, "Lithium metal anodes for rechargeable batteries," *Energy and Environmental Science*, vol. 7, no. 2, 2014, doi: 10.1039/C3EE40795K.

[48] N. Bensalah and H. Dawood, "Review on synthesis, characterizations, and electrochemical properties of cathode materials for lithium ion batteries," *Journal of Material Science & Engineering*, vol. 5, no. 4, 2016, doi: 10.4172/2169-0022.1000258.

[49] Y. Zheng, J. Hwang, K. Matsumoto, and R. Hagiwara, "Charge-discharge properties and reaction mechanism of cation-disordered rutile-type Li1.2MnFe1.2F6.8," *Electrochimica Acta*, vol. 405, 2022, Art. no. 139627, doi: 10.1016/j.electacta.2021.139627.